A Comparison Between a Time Domain and Continuous Wave Small Animal Optical Imaging System

Shay Keren, Olivier Gheysens, Craig S. Levin, and Sanjiv S. Gambhir*

***Abstract*—We present a phantom study to evaluate the performance of the eXplore Optix (Advanced Research Technologies-GE Healthcare), the first commercially available time-domain tomography system for small animal fluorescence imaging, and compare its capabilities with the widely used IVIS 200 (Xenogen Corporation-Caliper) continuous wave planar imaging system. The eXplore Optix, based on point-wise illumination and collection scheme, is found to be a log order more sensitive with significantly higher detection depth and spatial resolution as compared with the wide-area illumination IVIS 200 under the conditions tested. A time-resolved detection system allows the eXplore Optix to measure the arrival time distribution of fluorescence photons. This enables fluorescence lifetime measurement, absorption mapping, and estimation of fluorescent inclusion depth, which in turn is used by a reconstruction algorithm to calculate the volumetric distribution of the fluorophore concentration. An increased acquisition time and lack of ability to image multiple animals simultaneously are the main drawbacks of the eXplore Optix as compared with the IVIS 200.**

***Index Terms*—Fluorescence lifetime, molecular imaging, optical tomography, small animal imaging, time-domain imaging.**

I. Introduction

NONINVASIVE imaging of target-specific fluorescent probes in small animals is an emerging modality to identify molecular events with high specificity and sensitivity using nonionizing radiation in a cost and time effective way [1]. Recent developments in fluorescence imaging instrumentation allow researchers to better detect and localize weak signals emanating from tissues deep within living subjects [2]–[4].

Most often whole-body optical detection is performed by planar imaging using photographic principles to capture light emitted from animals [5], [6]. In recent years, noninvasive planar imaging has broadly affected biomedical research enabling *in vivo* visualization of molecular events such as gene expression and protein functions [1], [7], [8]. In conventional fluorescence planar imaging, the whole animal is illuminated with a broad beam of light tuned to the excitation wavelength of the fluorophore. Emitted fluorescent light is detected by a highly sensitive and low noise charged-coupled device (CCD) using an appropriate emission filter. Subsequently, a standard photographic image is acquired with white light illumination. Software superimposes both acquired images so the fluorescence signal topographic distribution can be deduced from the overlaid mouse photograph. Planar imaging is currently the most widely used approach for assessing the distribution of fluorescent probes *in vivo* due to its simple operation and inexpensive cost. However, planar imaging has inherent limitations in terms of fluorescent probe localization, quantification, and depth of detection, as explained below. Fluorescence intensity detected by a photographic method cannot be quantitated accurately since both fluorophore depth and concentration have similar effects on emerging light intensity distribution, which cannot be decoupled. In addition, planar imaging systems are limited to a detection depth of a few millimeters due to background fluorescence. This background fluorescence, mainly caused by autofluorescence, remains unattenuated since it is predominantly generated from superficial layers. In contrast, fluorescent light emerging from deep tissues is significantly attenuated by scattering and absorption. Recently developed planar imaging systems use spectral information to differentiate multiple fluorophores from background fluorescence, improving signal-to-background ratio, and hence sensitivity [9].

Driven by the need for deeper detection, better quantification, and accurate localization, new mathematical models describing photon propagation through tissues, and advanced illumination schemes have been developed enabling noninvasive fluorescence tomography, summarized in recently published reviews [2], [4], [10]. New generation optical tomography systems allow quantitative 3-D volumetric imaging of fluorescence distribution. There are currently three approaches for achieving optical tomography: continuous wave (CW), time domain (TD), and frequency domain (FD).

In CW fluorescence tomography, a constant intensity light source is illuminating points on the subject's surface and transmitted light is collected at different points on the surface surrounding the subject [11]. Measurements of both emission and excitation light can be collected between multiple source-detector pairs. All the measurements from the different projections are then combined into an inverse mathematical model to reconstruct the fluorophore volumetric distribution [12].

Manuscript received October 24, 2006; revised May 31, 2007. This work was supported in part by the NCI Center for Cancer Nanotechnology Excellence (CCNE) U54 CA119367 (SSG), in part by the NIBIB BRP (SSG), in part by In Vivo Cellular Molecular Imaging Center (ICMIC) under Grant P50 CA114747 (SSG), in part by NCI Small Animal Imaging Resource Program, and in part by FWO (OG). *Asterisk indicates corresponding author.*

S. Keren, O. Gheysens, and C. S. Levin are with the Molecular Imaging Program at Stanford (MIPS), Radiology Department, Stanford University, Stanford, CA 94305 USA (e-mail: shayk@stanford.edu; olivierg@stanford.edu; cslevin@stanford.edu).

*S. S. Gambhir is with the Molecular Imaging Program at Stanford (MIPS), Departments of Radiology and Bioengineering, Stanford University, Stanford, CA 94305 USA (e-mail: sgambhir@stanford.edu).

Digital Object Identifier 10.1109/TMI.2007.902800

0278-0062/$25.00 © 2007 IEEE

Authorized licensed use limited to: Stanford University. Downloaded on June 01,2010 at 22:33:46 UTC from IEEE Xplore. Restrictions apply.

In TD fluorescence tomography, the subject is illuminated with a short, subnanosecond duration laser pulse and a fast detector measures the arrival distribution of photons as a function of time at different locations [13]. A light pulse propagating through the tissue is broadened and attenuated due to scattering and absorption. A fluorophore embedded in tissue will be excited by this pulse of light and emit a fluorescence pulse with a lifetime decay typical to the fluorophore [14].

In FD technology, a light source with sine wave modulated intensity at radio-frequencies is illuminating the subject. Measurement of amplitude attenuation and phase delay of emitted fluorescence light, accumulates as it propagates through tissue, allow tomography of fluorescent sources [15]. A fluorophore excited with intensity modulated light will emit fluorescence at the same modulation frequency, with amplitude attenuation and phase shift resulting from its typical fluorescence lifetime. Light emerging from the surface is measured by a fast detector and a radio-frequency oscillator to drive the diode laser provides a reference signal for phase detection [16].

Comparison between the different optical tomography approaches is still largely under debate. Nevertheless, it can be said that CW and FD systems are relatively inexpensive, easy to develop, and use and can provide short time scans [17]. TD systems, on the other hand, tend to use photon counting detectors which are slow but highly sensitive. In addition to spatial intensity distribution, TD and FD systems can provide temporal information from which one can derive fluorescence lifetime [14], [18]. Fluorescence lifetime allows distinction between exogenous and endogenous fluorescence resulting in an increase of the signal-to-noise ratio, hence of the sensitivity. Moreover, this allows multiplexing of several fluorescent probes with different lifetimes, even if they have overlapping spectra. In addition, changes in the fluorescence lifetime of a particular fluorophore are a sensitive indicator of variations in the fluorophore microenvironment [19], [20]. With TD and FD techniques it is possible to independently measure the distribution of both scattering and absorption coefficients, an important information for accurate calculation of fluorophore concentration and location [21]. FD systems are less affected by ambient light by rejecting uncorrelated light using lock-in amplifiers [22].

Recently, the first TD small animal fluorescence imaging system, the eXplore Optix (Advanced Research Technologies-GE Healthcare, St. Laurent, QC, Canada), was commercially released. Here, we present a phantom study to assess the performance capabilities of the eXplore Optix TD imaging system and compare it with the well-known IVIS 200 planar CW imaging system (Xenogen Corporation-Caliper, Alameda, CA).

II. Methods and Materials

A. Instrumentation

TD Tomography System: The eXplore Optix system, described schematically in Fig. 1(a), uses a fixed pulsed laser diode as an illumination source with the following characteristics. Excitation occurs at a wavelength of 670 nm with pulse repetition rate of 80 MHz, pulse width of less than 100 ps, and a tunable average power of 0–500 μW by using a circular variable attenuator, achieving maximal peak power of about 62.5 mW. A galvomirror is used to perform a raster scan of the selected region of interest (ROI) with a step size ranging from 0.5 to 3 mm and a spot size of 1 mm at the image plane. A second galvomirror collects the emanating light, 3 mm away from the illumination point, through a 693-nm-long pass emission filter blocking light at the excitation wavelength with optical density (OD) 9. Subsequently, a photomultiplier tube (PMT) coupled to a time correlated single photon counting system collects the light allowing dynamic detection of the fluorescence signal with a temporal resolution of 250 ps. Dynamic range of PMT is 16 000, from a dark current level of 125 ph/s to a saturation value of 2 000 000 ph/s and its dead time is 125 ns. In addition, a second camera is incorporated into the system to perform a profilometric scan in order to obtain the topography of the animal. Data analysis and fluorescence lifetime parameters are obtained using the TD software of the system (eXplore Optix analysis workstation 1.00.00). A fluorescence lifetime map is obtained by fitting the tail of the photon temporal distribution curve and obtaining the characteristic decay time at each point. The eXplore Optix software package includes a 3-D concentration reconstruction algorithm that uses an iterative inverse solution to the Born approximation of the diffusion equation for photon density waves in a homogenous scattering medium [23].

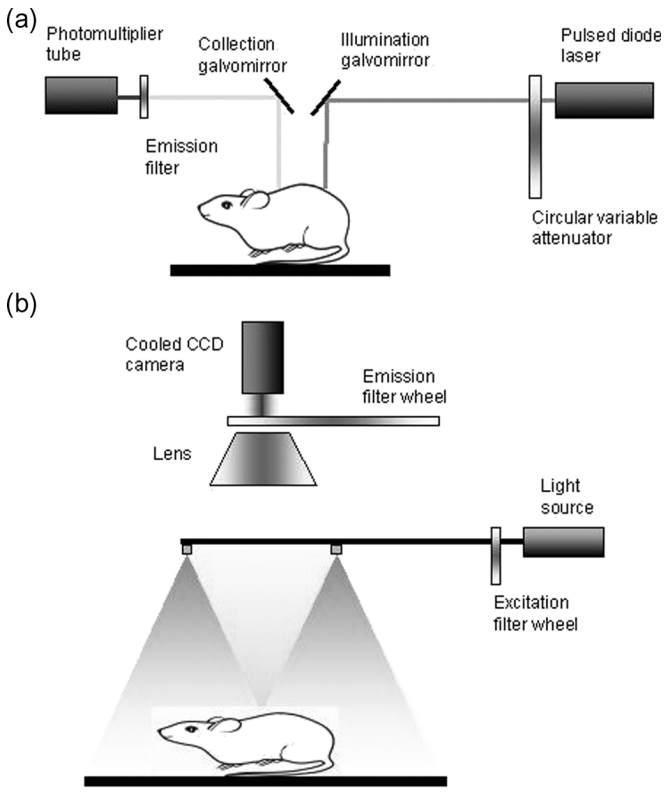

Fig. 1. Schematic description of the (a) eXplore Optix TD imaging system and the (b) IVIS 200 planar CW imaging system.

Recently, Advanced Research Technologies released a new model, named eXplore Optix MX, with four different excitation lasers and an emission filter wheel allowing imaging of several fluorophores.

Authorized licensed use limited to: Stanford University. Downloaded on June 01,2010 at 22:33:46 UTC from IEEE Xplore. Restrictions apply.

In this study, images on the eXplore Optix were acquired with the following parameters, chosen to achieve best results: topographic scan, 2-D scan ROI with 1-mm step size unless mentioned otherwise, point integration time 0.1–1 s and laser power of 100–500 μW depending on fluorophore concentration.

Planar Imaging System: The IVIS 200 system, originally designed for bioluminescence imaging and later adopted for fluorescence imaging, uses a CW quartz halogen lamp generating a constant 150-W broadband light that simultaneously and uniformly illuminates the whole field of view, as shown schematically in Fig. 1(b). The light is spectrally filtered for fluorescence excitation with an integrated 12-position excitation wheel. Fluorescent light is collected through a 24-position emission filter wheel with optical density OD 9 at excitation wavelength, and imaged by a f/.95–f/16, 50-mm lens on a low noise, 25 mm square back-thinned, 20-μm square pixel, 1024 $\times$ 1024 pixels imaging and cryogenically cooled (to $-105\,^{\circ}\mathrm{C}$), 16 bit CCD camera with minimum detectable luminance of $< 100\ \mathrm{photons/s/sr/cm^2}$. Five interchangeable lenses adjust the field of view, 4–26 cm, between high-resolution and high-throughput applications. Image analysis is performed by the system software (Living Image 2.5).

Xenogen has recently released a software package, termed Living Image 3-D, for more accurate reconstruction of concentration and location based on bioluminescence spectral imaging technique. Development of similar software for fluorescence imaging is currently under way.

In the current study, images on the IVIS 200 were taken with the following parameters, chosen to achieve best results: excitation filter Cy 5.5 (615–665 nm), emission filter Cy 5.5 (695–770 nm), fluorescence level high, binning medium (two pixels), field-of-view 6.4–12.3 cm depending on object size, f-number 2, exposure time 1–10 s depending on concentration.

B. Phantom Materials

The liquid phantom is composed of 1% Liposyn II (Abbott Laboratories) with a scattering coefficient, $\mu_{\mathrm{s}}' = 1\ \mathrm{mm^{-1}}$ [24], similar to that of tissue [25] and with negligible absorption. Absorption was introduced by India ink (Higgins, Sanford) with a measured absorption coefficient of $0.3016\ \mathrm{mm^{-1}}$ for a 0.1% concentration at a wavelength of 700 nm. Ink concentration is varied between 0–0.016% which is equivalent to $\mu_{\mathrm{a}} = 0 - 0.048\ \mathrm{mm^{-1}}$, resembling the typical absorption coefficient range measured in different tissues [25].

III. Results

A. Sensitivity and Linearity

The lowest detectable concentration of a fluorophore at the surface is an objective test to evaluate a system's sensitivity in the best case scenario with no absorption, scattering or autofluorescence. Here, we prepared serial dilutions in triplicates of Cy 5.5 in water (Amersham Bioscience) in a 96-well assay black plate (Corning Inc.). Signal-to-background ratio, where background level is the fluorescence signal measured in wells containing only water, as a function of Cy 5.5 concentration ranging from 0 to 1000 nM in a volume of 50 μl is shown in Fig. 2. Minimal detectable concentration is defined here as the highest concentration having a signal-to-noise ratio of one. The eXplore Optix shows a log order increase in minimal detectable concentration, 0.1 nM compared to 1 nM obtained using the IVIS 200, as can be seen on the log–log scale where signal to background level reaches just above 1. This is also the improvement ratio between the two imaging systems for the signal to noise ratio, above 10 nM concentration. Error bars indicate intensity standard deviation at every triplicate containing the same Cy 5.5 concentration. Signal-to-background standard deviation of background signal is ± 0.06 and ± 0.13 for IVIS 200 and eXplore Optix, respectively. Fluorescence intensity shows high linear correlation with Cy 5.5 concentration for more than 3 log orders of magnitude in both imaging systems. However, IVIS 200 readout shows higher linearity of fluorescence intensity as function of concentration with $R^2 = 0.998$, compared with $R^2 = 0.996$ for the eXplore Optix. Also, the IVIS 200 intensity seems more stable than the eXplore Optix as indicated by the standard deviation error bars.

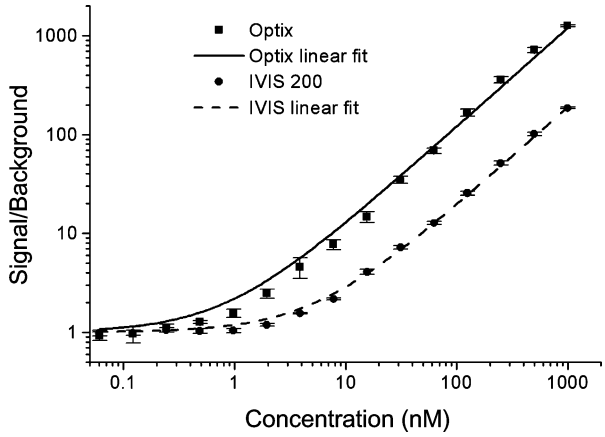

Fig. 2. Signal-to-noise ratio versus Cy 5.5 concentration measured by both eXplore Optix (square) and IVIS 200 (circle), plotted on a log–log scale. Both imaging systems show high correlation to their linear fit, however, the IVIS 200 shows a slightly better fit and lower standard deviation variations.

B. Depth of Detection

Evaluation of the largest depth for detecting a signal provides a good estimate of the imaging capabilities in deep tissues. A liquid phantom was constructed of a cylindrical container filled with Liposyn and India ink composition, simulating tissue scattering, and absorption coefficients, as described above. A 10 μl inclusion of 50 nM Cy 5.5 with a diameter of 3 mm was placed at the bottom of the container and the liquid level was changed to obtain different depths, with accuracy of ± 0.1 mm. Fig. 3(a) shows the maximal depth for signal detection as a function of absorption coefficient, varied by changing the ink concentration, measured by the eXplore Optix and the IVIS 200. Maximal detection depth is defined here as the depth where signal-to-background ratio approaches 1.2. Below that value the fluorescence image was too blurred to indicate the existence of fluorescence inclusion. As can be seen, maximal depth, with no addition of ink, of 10 mm is obtained using the eXplore Optix system compared with 5 mm maximal depth obtained using the IVIS 200 with an identical phantom. Yet for compositions simulating

Authorized licensed use limited to: Stanford University. Downloaded on June 01,2010 at 22:33:46 UTC from IEEE Xplore. Restrictions apply.

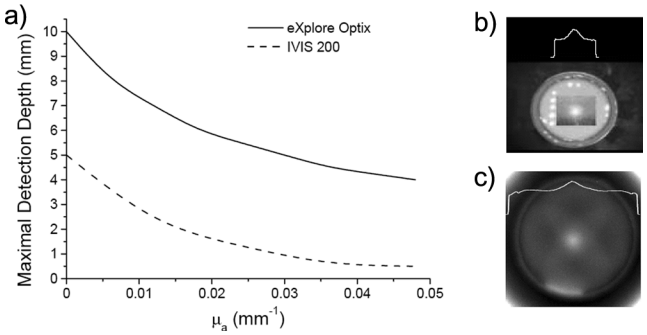

Fig. 3. (a) Maximal detection depth of a 10 μl inclusion of 50 nM Cy 5.5 as a function of absorption coefficient obtained by eXplore Optix (solid line) and IVIS 200 (dashed line). (b) Fluorescence distribution of an inclusion at 6 mm depth with $\mu_a = 0.024\ \mathrm{mm}^{-1}$ and its cross section taken by the eXplore Optix and (c) fluorescence distribution of an inclusion at 1.3 mm depth with $\mu_a = 0.024\ \mathrm{mm}^{-1}$ and its cross section taken by the IVIS 200.

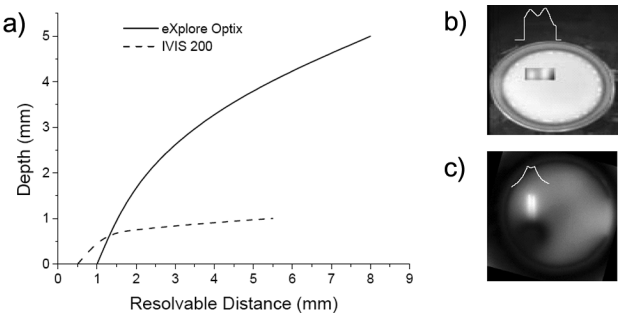

Fig. 4. (a) Resolvable depth of two 0.5 mm diameter capillary tubes filled with 2 μl volume of 50 nM Cy 5.5 as a function of tube separation distance obtained by eXplore Optix (solid line) and IVIS 200 (dashed line). (b) Fluorescence distribution of two capillary tubes at 5 mm depth and separation of 8 mm with its cross section taken by the eXplore Optix and (c) fluorescence distribution of two capillary tubes at 0.67 mm depth and separation of 2 mm with its cross section taken by the IVIS 200.

high absorbing tissues, the eXplore Optix could image the inclusion at 4 mm deep compared with only 0.5 mm obtained using the IVIS 200. Fig. 3(b) and (c) shows typical examples of the fluorescence distribution and cross section obtained using the eXplore Optix and the IVIS 200, respectively.

C. Spatial Resolution

Strong light scattering by tissues is the limiting factor on spatial resolution in fluorescence imaging resulting in poor size quantification of target [26]. Here, we measure the spatial resolution of both the eXplore Optix and the IVIS 200 by placing two capillary tubes, with 0.5 mm inner diameter and 0.2 mm wall thickness, each filled with 2 μl volume of 50 nM Cy 5.5 in liquid simulating tissue scattering properties and no absorption. For a given separation distance of the tubes, their depth is increased until fluorescence intensity between the tubes reached 90% of peak value. Above that value, signal from different tubes can not be visually separated. Fig. 4(a) shows the maximal resolvable distance as a function of depth for both the eXplore Optix and IVIS 200. As can be seen, at the surface the IVIS 200 spatial resolution, 0.5 mm, exceeds the eXplore Optix resolution which is limited by the optical system spot size to 1 mm. However, beyond a depth of 1 mm, the eXplore Optix resolution is significantly better than that of the IVIS 200. The eXplore Optix can resolve features separated by 8 mm apart at a depth of 5 mm, whereas on the IVIS 200 the same resolution is lost beyond a depth of 1 mm. Fig. 4(b) and (c) shows typical examples of the fluorescence distribution and cross section obtained using the eXplore Optix and the IVIS 200, respectively.

D. Depth and Concentration Estimation

Inclusion depth and concentration are estimated by the eXplore Optix software using arrival time of fluorescent emission. To test the accuracy of software depth and concentration estimate and the validity of a monotonic relation between inclusion depth and photon pulse arrival time, we measure the temporal point spread function generated by 10 μl volume of 50 nM Cy 5.5 inclusion placed at different depths in liquid phantom simulating scattering properties of tissues without light absorbing ink. Fig. 5(a) shows the estimated depth and concentration, calculated by the eXplore Optix software as a function of the actual depth. As can be seen both estimates are far from accurate, although estimated depth is correlated with actual depth until 4 mm, the depth value it self is poorly estimated. Estimate of concentration is decreasing as depth increases were it is expected to stay constant. Fig. 5(b) shows the depth dependence of the mean, median and peak arrival time of fluorescence signal. Error bars indicate timing standard deviation of nine points around the most intense pixel. As expected, mean arrival time increases monotonically with increased depth [27] and so does the median arrival time. On the other hand, the peak arrival time monotonically increases up to 6 mm, after that peak arrival time decreases and becomes more affected by noise as indicated by increased error bars.

E. Volumetric Fluorophore Concentration Reconstruction

One of the unique features of the eXplore Optix tomography system is its ability to reconstruct a 3-D intensity distribution. An example is shown in Fig. 6(a), where four Cy 5.5 inclusions at different starting depths, 0, 2, 5, and 8 mm (all have Cy 5.5 concentration 10 nM) in upper row, and four Cy 5.5 inclusions of different concentrations, 5, 10, 20, and 50 nM (all are at depth of 2 mm) in lower row, are buried in a solid phantom slab, shown schematically in Fig. 6(b). The dimensions of the cylindrical fluorescence inclusions are 4 mm in diameter and 3 mm thick. The optical properties of solid phantom slab $\mu_s' = 1\ \mathrm{mm}^{-1}$ and $\mu_a = 0.053\ \mathrm{mm}^{-1}$. The reconstructed image in Fig. 6(a) shows two inclusions at slightly different depth, upper row, and three inclusions with different concentration, lower row, superimposed on a profilometry image of the solid phantom slab. In the iso-contour representation used by the software, higher fluorescence intensity is represented by a larger size reconstructed inclusion. As can be seen, inclusions with the same concentration and depth, second inclusion from right in upper row and third inclusion from left in lower row, have the same reconstructed size. Quantitative measurements on the volumetric representation are not possible in current software version. All inclusions could not be imaged together since higher laser power would saturate the PMT at the high concentration inclusion; therefore, laser average power was set to 118 μW.

Authorized licensed use limited to: Stanford University. Downloaded on June 01,2010 at 22:33:46 UTC from IEEE Xplore. Restrictions apply.

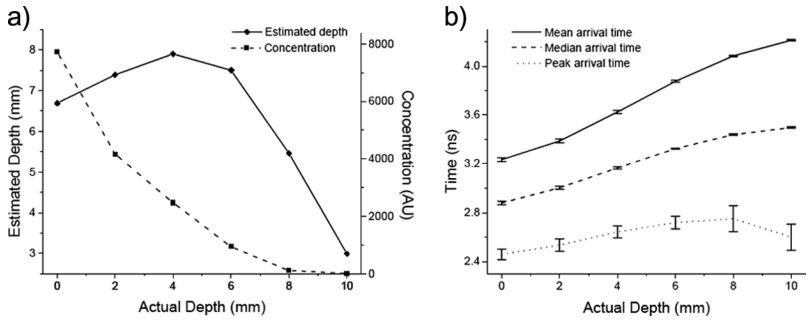

Fig. 5. (a) Depth (solid line) and concentration (dashed line) estimated by eXplore Optix software as function of actual inclusion depth. (b) Fluorescence mean, median, and peak arrival time as function of actual inclusion depth obtained by eXplore Optix.

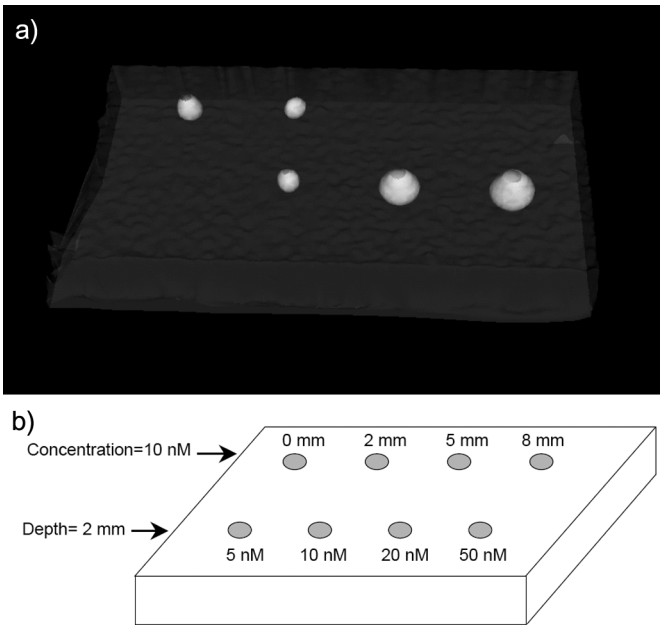

Fig. 6. Volumetric concentration reconstruction of a solid phantom containing Cy 5.5 inclusions with different concentrations and at different depths obtained by eXplore Optix. (a) Reconstructed concentration, shown as white spheres, superimposed on profilometry image and (b) a schematic description of the solid phantom.

IV. Summary

The eXplore Optix is found to be log order more sensitive at detecting minute concentrations of Cy 5.5 and has a similar improvement in signal to noise ratio compared with the IVIS 200. The depth at which Cy 5.5 fluorescence can be detected using the eXplore Optix is significantly larger compared with that of the IVIS 200 system. Spatial resolution is another criterion showing great improvement for tomography compared with planar imaging. These results are a consequence from the two distinct illumination methods used by the different imaging systems. Wide-area illumination used by IVIS 200 delivers much less power to the examined ROI compared with point wise illumination used by eXplore Optix. Furthermore, in wide-area illumination, the detected signal contains spatially integrated information, resulting in degradation of spatial resolution. However, the different filter setting in the two systems had negligible effect on the results when imaging Cy 5.5. Depth estimation and the concentration reconstruction algorithm of the eXplore Optix gives poor results in phantom studies, probably due to simplified algorithm that calculates depth from fluorescence emission peak arrival time. Moreover, the algorithm is currently using premeasured phantom properties to achieve those results. The need to use postulated values will likely further decrease the accuracy of the concentration reconstruction in heterogeneous animals. In addition, the 3-D fluorescence reconstruction algorithm is based on the diffusion approximation which gives large error when the distance from the boundary is not much larger than the transport mean free path [27]. Accompanied with a rigorous tomographic reconstruction model, possibly by combining information from complimentary modalities, TD fluorescence tomography shows promise to recover the shape, location and concentration of fluorescent inclusions in three-dimensions in living animals with great accuracy. The major drawbacks of the eXplore Optix system is the longer acquisition time and the inability to scan multiple subjects at the same time. The scan time of three rows of 12 wells using the eXplore Optix ranges from 5 to 50 min, depending on integration time 0.1–1 s, compared to 1 min using the IVIS 200. High throughput is essential in studies where large number of animals is used. Moreover, high temporal resolution may be required when building kinetic data of fluorophore distribution and the eXplore Optix allows pharmacokinetic follow-up of only a limited area. The IVIS 200 showed higher signal linearity with concentration and lower intensity variations between samples compared with the eXplore Optix as a result of up to 10% dead time of the eXplore Optix detection path at high photon flux. The results shown in this paper and the conclusion drawn from these results are relevant for the specific systems that were used under the given conditions, with modifications to those imaging systems and different experiments one might arrive at different conclusions. The current phantom study is still far from representing a realistic living animal; autofluorescence, respiratory motion, and heterogeneous structure present greater challenges for *in vivo* optical imaging systems and will result in lower sensitivity poorer depth of detection and resolution as stated in this phantom study. The eXplore Optix allows gating of the intensity signal by its fluorescence lifetime, this feature should significantly increase sensitivity by discriminating between dye and autofluorescence signals. Further studies with phantoms containing background fluorescence and small animals should be performed for evaluating the effect of background autofluorescence. The development of the eXplore Optix TD imaging system takes an important step forward in

Authorized licensed use limited to: Stanford University. Downloaded on June 01,2010 at 22:33:46 UTC from IEEE Xplore. Restrictions apply.

whole-body small animal fluorescence imaging techniques to advance it from a qualitative tool to a volumetric representation of the fluorophore concentration distribution.

REFERENCES

[1] T. F. Massoud and S. S. Gambhir, "Molecular imaging in living subjects: Seeing fundamental biological processes in a new light," *Genes Development*, vol. 17, pp. 545–580, 2003.

[2] V. Ntziachristos, J. Ripoll, L. V. Wang, and R. Weissleder, "Looking and listening to light: The evolution of whole-body photonic imaging," *Nat. Biotechnol.*, vol. 23, pp. 313–320, 2005.

[3] M. Gurfinkel, S. Ke, X. Wen, C. Li, and E. M. Sevick-Muraca, "Near-infrared fluorescence optical imaging and tomography," *Disease Markers*, vol. 19, pp. 107–121, 2003, 2004.

[4] A. P. Gibson, J. C. Hebden, and S. R. Arridge, "Recent advances in diffuse optical imaging," *Phys. Med. Biol.*, vol. 50, pp. R1–R43, 2005.

[5] U. Mahmood, C. H. Tung, A. Bogdanov, and R. Weissleder, "Near-infrared optical imaging of protease activity for tumor detection," *Radiology*, vol. 213, pp. 866–870, 1999.

[6] M. Yang, E. Baranov, P. Jiang, F. X. Sun, X. M. Li, L. Li, S. Hasegawa, M. Bouvet, M. Al-Tuwaijri, T. Chishima, H. Shimada, A. R. Moossa, S. Penman, and R. M. Hoffman, "Whole-body optical imaging of green fluorescent protein-expressing tumors and metastases," *Proc. Nat. Acad. Sci. USA*, vol. 97, pp. 1206–1211, 2000.

[7] H. R. Herschman, "Molecular imaging: Looking at problems, seeing solutions," *Science*, vol. 302, pp. 605–608, 2003.

[8] R. Weissleder and V. Ntziachristos, "Shedding light onto live molecular targets," *Nat. Med.*, vol. 9, pp. 123–128, 2003.

[9] X. Gao, Y. Cui, R. M. Levenson, L. W. K. Chung, and S. Nie, "*In vivo*cancer targeting and imaging with semiconductor quantum dots," *Nat. Biotechnol.*, vol. 22, pp. 969–976, 2004.

[10] A. H. Hielscher, "Optical tomography imaging of small animals," *Current Opinion Biotechnol.*, vol. 16, pp. 79–88, 2005.

[11] E. Graves, J. Ripoll, R. Wissleder, and V. Ntziachristos, "Sub-millimeter resolution fluorescence molecular imaging system for small animal imaging," *Med. Phys.*, vol. 30, pp. 901–911, 2003.

[12] V. Ntziachristos and R. Weissleder, "Experimental three dimensional fluorescence reconstruction of diffuse media using a normalized Born approximation," *Opt. Lett.*, vol. 26, pp. 893–895, 2001.

[13] S. Bloch, F. Lesage, L. McIntosh, A. Gandjbakhche, K. Liang, and S. Achilefu, "Whole-body fluorescence lifetime imaging of a tumor-targeted near-infrared molecular probe in mice," *J. Biomed. Opt.*, vol. 10, pp. 054003 1–054003 8, 2005.

[14] D. Elson, J. Requejo-Isidro, I. Munro, F. Reavell, J. Siegel, K. Suhling, P. Tadrous, R. Benninger, P. Lanigan, J. McGinty, C. Talbot, B. Treanor, S. Webb, A. Sandison, A. Wallace, D. Davis, J. Lever, M. Neil, D. Phillips, G. Stamp, and P. French, "Time-domain fluorescence lifetime imaging applied to biological tissue," *Photochem. Photobiol. Sci.*, vol. 3, pp. 795–801, 2004.

[15] J. Lee and E. M. Sevick-Muraca, "Three-dimensional fluorescence enhanced optical tomography using referenced frequency-domain photon migration at emission and excitation wavelengths," *J. Opt. Soc. Am. A*, vol. 19, pp. 759–770, 2002.

[16] A. Godavarty, A. J. Eppstein, C. Zhang, S. Theru, A. B. Thompson, M. Gurfinkel, and E. M. Sevick-Muraca, "Fluorescence-enhanced optical imaging in large tissue volumes using a gain-modulated ICCD camera," *Phys. Med. Biol.*, vol. 48, pp. 1701–1720, 2003.

[17] C. H. Schmitz, M. Löcker, J. M. Lasker, A. H. Hielscher, and R. L. Barbour, "Instrumentation for fast functional optical tomography," *Rev. Sci. Instrum.*, vol. 73, pp. 429–439, 2002.

[18] M. A. O'Leary, D. A. Boas, X. D. Li, B. Chance, and A. G. Yodh, "Fluorescence lifetime imaging in turbid media," *Opt. Lett.*, vol. 21, pp. 158–160, 1996.

[19] K. Suhling, J. Siegel, D. Phollips, P. M. W. French, S. Leveque-Fort, S. E. D. Webb, and D. M. Davis, "Imaging the environment of green fluorescent protein," *Biophys. J.*, vol. 83, pp. 3589–3595, 2002.

[20] E. Kuwana and E. M. Sevick-Muraca, "Fluorescence lifetime spectroscopy for pH sensing in scattering media," *Anal. Chem.*, vol. 75, pp. 4325–4329, 2003.

[21] S. R. Arridge and W. R. B. Lionheart, "Nonuniqueness in diffusion-based optical tomography," *Opt. Lett.*, vol. 23, pp. 882–884, 1998.

[22] J. P. Houston, A. B. Thompson, M. Gurfinkel, and E. M. Sevick-Muraca, "Sensitivity and depth penetration of continuous wave versus frequency-domain photon migration near-infrared fluorescence contrast-enhanced imaging," *Photochem. Photobiol.*, vol. 77, pp. 420–430, 2003.

[23] S. Lam, F. Lesage, and X. Intes, "Time domain fluorescent diffuse optical tomography: Analytical expressions," *Opt. Exp.*, vol. 13, pp. 2263–2275, 2005.

[24] A. Godavarty, E. M. Sevick-Muraca, and M. J. Eppstein, "Three-dimensional fluorescence lifetime tomography," *Med. Phys.*, vol. 32, pp. 992–1000, 2005.

[25] J. Mobley and T. Vo-Dinh, "Optical properties of tissues," in *Biomedical Photonics Handbook*. Boca Raton, FL: CRC Press, 2003, ch. 2.

[26] V. Chernomordik, A. Gandjbakhche, M. Lepore, R. Esposito, and I. Delfino, "Depth dependence of the analytical expression for the width of the point spread function (spatial resolution) in time-resolved transillumination," *J. Biomed. Opt.*, vol. 6, pp. 441–445, 2001.

[27] K. M. Yoo, F. Liu, and R. R. Alfano, "When does the diffusion approximation fail to describe photon transport in random media?," *Phys. Rev. Lett.*, vol. 64, pp. 2647–2650, 1990.

Authorized licensed use limited to: Stanford University. Downloaded on June 01,2010 at 22:33:46 UTC from IEEE Xplore. Restrictions apply.